J Am Oil Chem Soc (2013) 90:1049–1062
DOI 10.1007/s11746-013-2253-9

ORIGINAL PAPER

The Experimental Observation and Modelling of Film Thinning and Film Retraction during the Interfacial Coalescence of Biodiesel and Glycerol Droplets

A. Abeynaike · J. F. Davidson · M. R. Mackley

Received: 11 November 2012 / Revised: 2 April 2013 / Accepted: 8 April 2013 / Published online: 12 May 2013

Abstract This paper is concerned with the way interfacial coalescence of a single drop of biodiesel or glycerol occurs at a glycerol/biodiesel interface. Two stages of interfacial coalescence were studied: the thinning of the trapped liquid film between the rising or falling droplet and bulk fluid interface, and the retraction of the film after the film had ruptured. Unexpectedly, the thinning time for the high viscosity glycerol film around a rising biodiesel droplet was found to be much shorter than that for a low viscosity biodiesel film around a sedimenting glycerol droplet. Squeeze flow modelling showed that the film of glycerol around a biodiesel droplet was bounded by relatively inviscid biodiesel and therefore flowed with high slip at its interfaces, resulting in rapid film thinning. The biodiesel film around a glycerol droplet was bounded by highly viscous glycerol and flowed with little slip at the interfaces, resulting in slower film thinning. After rupture, film retraction was found to be much faster for biodiesel droplets than for glycerol droplets. The drag exerted by the fluid surrounding the film was found to control the retraction kinetics. The results are of particular relevance to the separation of glycerol from biodiesel and of general relevance to coalescence kinetics for immiscible drops at an interface.

Keywords Coalescence · Droplets · Film thinning · Film drainage · Film retraction

List of symbols

a	Radius of the rim at the edge of a retracting film (m)
A	Area (for example, of a film or interface) (m^2)
b	Half the width of a droplet at a liquid/liquid interface (m)
c	Half the height of a droplet at a liquid/liquid interface (m)
d	Droplet diameter (m)
F	Force (N)
F_D	External drag force exerted by surrounding fluid (N)
g	Acceleration due to gravity (m/s^2)
h	$H/2$ (m)
H	Thickness of a liquid film (m)
H_0	Initial thickness of a liquid film (m)
L	Distance travelled by rim (see Fig. 13) (m)
p	Pressure or axial stress (Pa)
p_{rr}	Axial stress in the r direction (Pa)
p_{xx}	Axial stress in the x direction (Pa)
p_{zz}	Axial stress in the z direction (Pa)
Δp	Pressure difference (Pa)
r	Radius; radial dimension (m)
r_c	Radius of curvature of the film around a droplet (m)
r_h	Radius of droplet in the plane $z = 0$ (see supplementary material)
r_i	Initial radius of a droplet before reaching a liquid/liquid interface (m)

Electronic supplementary material The online version of this article (doi:10.1007/s11746-013-2253-9) contains supplementary material, which is available to authorised users.

A. Abeynaike (✉) · J. F. Davidson · M. R. Mackley
Department of Chemical Engineering and Biotechnology, University of Cambridge, Pembroke Street, Cambridge CB2 3RA, UK
e-mail: arjan.abeynaike@cantab.net

Present Address:
A. Abeynaike
BP Chemicals Ltd, Hull HU12 8DS, UK

R	Radius of plates in squeeze flow model (see Fig. 2) (m)
Re	Reynolds number of a film
t	Time (s)
u	Velocity (m/s)
u_{rim}	Velocity of a rim on a film retracting around a droplet at a liquid/liquid interface (m/s)
V	Droplet volume (m^3)
x	Horizontal distance (m)
x_1, x_2	Horizontal distance at times 1 and 2
z	Vertical distance (m)

Greek symbols

$\dot{\varepsilon}_{rr}$	Strain rate in the radial direction
$\dot{\varepsilon}_{zz}$	Strain rate in the vertical direction
θ	Angle (rad)
μ	Viscosity (Pa·s)
μ_d	Droplet phase viscosity (Pa·s)
μ_f	Film viscosity (Pa·s)
ρ_d	Droplet phase density (kg/m^3)
ρ_f	Film density (kg/m^3)
$\Delta\rho$	$\rho_f - \rho_d$ (kg/m^3)
σ	Interfacial tension (N/m)
τ	Shear stress (Pa)

Introduction

Interfacial coalescence involves the approach and incorporation with the bulk phase of a droplet at a horizontal liquid/liquid interface [1]. Interfacial coalescence is important in the separation of liquid/liquid dispersions as it allows droplets to be incorporated into a continuous phase, which can then be removed from the dispersion. When producing biodiesel by the transesterification reaction, the product contains glycerol droplets dispersed within a continuous phase of biodiesel [2]. One method of separating the denser glycerol is by gravity sedimentation, which results in a continuous bottom layer of glycerol [2]. The way in which glycerol droplets coalesce to form a continuous phase is therefore relevant to biodiesel production. The system also makes a suitable candidate for optical interrogation of the process, as there is good optical contrast between the two fluids.

There are five main steps to interfacial coalescence [1]:

1. Approach of the droplet to the interface.
2. Thinning of a "trapped" liquid film that separates the droplet from the continuous phase.
3. Rupture of the trapped film.
4. Retraction of the ruptured film around the droplet.
5. Movement of the droplet into its own continuous phase (called the homophase).

This paper is concerned with steps 2 and 4.

Thinning of the Liquid Film Between a Droplet and Its Homophase

When a droplet approaches a liquid/liquid interface, the liquid between the droplet and the interface forms a thin film. The liquid flows out of the film under the weight (or buoyancy) of the droplet, as shown in Fig. 1a for a biodiesel droplet and Fig. 1b for a glycerol droplet. The film gradually reduces in thickness until it eventually ruptures, allowing the droplet to move into the homophase. Film thinning is the rate limiting step of interfacial coalescence, as the other steps (film retraction and flow into the homophase) occur much faster [1].

Film thinning may be modelled as the flow of a fluid between two interfaces that are pressed together under a given force. Such flow is called squeeze flow and has been modelled for a range of fluid types [3]. In a standard squeeze flow scenario, fluid is placed between two flat circular plates which are brought together under a constant force, as shown in Fig. 2.

The variation of H, the distance between the plates, with time can be derived from the mass balance, force balance on a fluid element, rheology of the fluid and force balance on the plate. The mass balance at any radial position r is described by:

$$-\frac{dh}{dt}\pi r^2 = 2\pi r \int_o^h u dz \tag{1}$$

where u is the velocity of the fluid in the r direction and $h = H/2$. A force balance on a fluid element yields:

$$\frac{\partial \tau}{\partial z} = \frac{\partial p}{\partial r} \tag{2}$$

where τ is the shear stress and p is the fluid pressure. The rheological equation for a Newtonian fluid is:

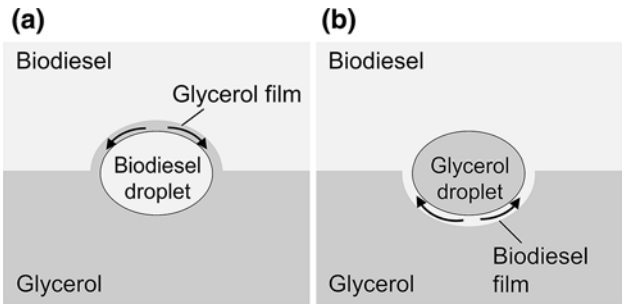

Fig. 1 Schematic diagram of droplets at the liquid/liquid interface during the film thinning stage: **a** a rising biodiesel droplet and **b** a falling glycerol droplet

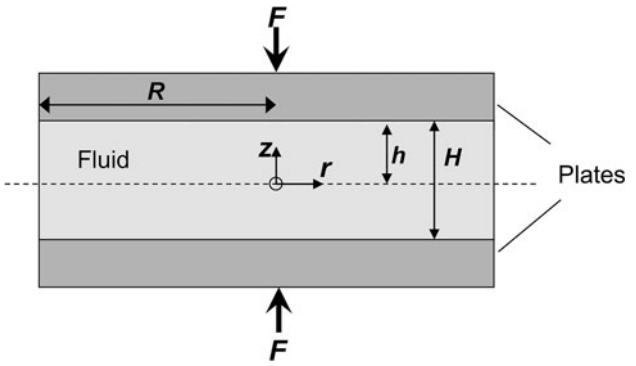

Fig. 2 Schematic diagram of a standard scenario for squeeze flow, whereby a fluid is squeezed under a force F between two parallel solid circular plates of radius R

$$\tau = \mu_f \frac{du}{dz} \tag{3}$$

where μ_f is the film viscosity. A force balance may be performed over the area of the plate, assuming inertial effects are negligible, such that:

$$F = \int_0^R 2\pi r \Delta p dr \tag{4}$$

where Δp is the difference between the pressure at point r and the pressure external to the squeezed fluid. Eqs. (1), (2), (3) and (4) may be solved using the boundary conditions of $\frac{\partial u}{\partial z} = 0$ at $z = 0$ (which assumes symmetry about the centre line), $u = 0$ at $z = h$ (i.e. no fluid velocity at the wall), and the initial condition $h = h_0$. The result is then [4]:

$$H(t) = H_0 \left(1 + \frac{4H_0^2 Ft}{3\pi\mu_f R^4}\right)^{-\frac{1}{2}} \tag{5}$$

where H_0 is the initial distance between the plates. Eq. (5) holds true where the material on either side of the liquid film is solid, so that a condition of no slip can be assumed at the boundaries of the film, i.e. fluid velocity is zero at the interfaces. In this case the "no slip" boundary conditions result in transverse velocity profile development across the film thickness and the resulting parabolic velocity profile leads to simple shear forces retarding the thinning process. For "no slip" boundary conditions, it is normal to ignore the weaker extensional viscosity terms due to radial velocity changes.

Instead of the no slip boundary condition, the "perfect slip" boundary condition may be assumed (i.e. the interface is completely mobile and so presents no resistance to motion). In this case the function $H(t)$ may be derived by considering the mass balance, axial stresses on a fluid element and a force balance on the plate. As there is no resistance at the fluid interface, the velocity of the fluid u in the radial direction is assumed to be uniform for all values of h. The mass balance is then:

$$-\frac{dH}{dt}\pi r^2 = 2\pi r u H \tag{6}$$

The axial stress in the radial direction, p_{rr}, is given by (5):

$$p_{rr} = -p + 2\mu_f \dot{\varepsilon}_{rr} = -p + 2\mu_f \frac{du}{dr} \tag{7}$$

where $\dot{\varepsilon}_{rr}$ is the strain rate in the radial direction and p is the static pressure external to the squeezed fluid. Differentiating Eq. (6) with respect to r, and substituting into Eq. (7) gives:

$$p_{rr} = -p - \frac{\mu_f}{H}\frac{dH}{dt} \tag{8}$$

The axial stress in the vertical z direction, p_{zz}, is given by (5):

$$p_{zz} = -p + 2\mu_f \dot{\varepsilon}_{zz} = -p + \frac{2\mu_f}{H}\frac{dH}{dt} \tag{9}$$

Assuming $p_{rr} = 0$, as there is no resistance at the boundaries, then:

$$p_{zz} = \frac{3\mu_f}{H}\frac{dH}{dt} \tag{10}$$

Assuming inertial effects are negligible, a force balance on the plate is simply:

$$F = -p_{zz} A \tag{11}$$

where A is the plate area. Substituting Eq. (10) into Eq. (11) gives (3):

$$H(t) = H_0 \exp(-Ft/3\mu_f A) \tag{12}$$

In this case, the resistance to flow is a consequence of the radial extensional deformation and the "weak" extensional viscosity is the mechanism for the resisting force.

The two extreme model boundary conditions for squeeze flow ("no slip" and "perfect slip") are used to describe film thinning in this paper. In the case of a biodiesel droplet approaching the interface, a high viscosity glycerol film is trapped between the low viscosity biodiesel droplet and the biodiesel homophase (as in Fig. 1a). In this situation the low viscosity of the liquid surrounding the film provides a boundary which is equivalent to the "perfect slip" boundary condition for squeeze flow. In the case of a glycerol droplet approaching an interface (Fig. 1b), a biodiesel film is sandwiched between high viscosity glycerol, which is equivalent to the "no slip" squeeze flow boundary condition.

The squeeze flow models have been used by many previous authors to describe film thinning in droplet

coalescence, often with some modification (for example [6–10]). Many studies have preferred to use the no slip condition for all systems, even for bubble coalescence. It is often stated that trace amounts of surfactants, which are always present unless the materials are extremely clean, will create an immobile interface, and that therefore the no slip condition is valid [11–13]. Despite this view, mobile and partially mobile interfaces have also been modelled [7, 12]. In a refinement to the simple flat film model, the curvature of the film has been considered [11, 14].

Besides the fluid mechanics of film thinning, other factors that have been investigated included mass transfer, surfactants and electrostatic forces. Several studies investigated the effect of mass transfer on film thinning [15–17]. Mass transfer of a solute from the droplet into the surrounding material results in a higher concentration of the solute in the film than in the droplet phase. The resulting gradient in interfacial tension enhances the film thinning due to the Marangoni effect. The presence of surfactants in the film is also expected to affect film thinning [6, 18–21]. As the film thins, the film becomes depleted of surfactant compared to the droplet phase. The reduced surfactant concentration in the film creates an interfacial tension gradient that inhibits further film thinning because of the Marangoni effect. This mechanism of coalescence inhibition is thought to be behind the Bancroft rule, which states that a stable emulsion can be formed when the surfactant preferentially dissolves in the continuous phase [18]. The effects of the disjoining pressure [17, 18], which results from the interaction of electric double layers, and van der Waals forces [11, 22] have also been included in film thinning models.

Despite the significant body of work on modelling film thinning, prediction of experimental results is still difficult. One reason for this is that the results from identical coalescence experiments often vary widely. Many experimental studies have measured the time between a droplet arriving at an interface and rupture of the thin film [9, 10, 23–25]. These measurements show that very wide ranges of film thinning times are exhibited by any one system, typically from ones to tens of seconds. Furthermore, the times do not follow a predictable normal distribution about a mean. The main reason for the variation in coalescence times is that the rupture of the film will not occur every time at a certain film thickness, but the probability of rupture may increase as the film thins and becomes more susceptible to random thermal or mechanical disturbances [9, 18]. A simple squeeze flow film thinning model cannot capture these disturbances, which appear to play an important role in film rupture. Equations (5), (12) asymptote towards $H = 0$ as $t \rightarrow \infty$. Therefore, to determine the time required for a film to thin to the point of rupture, a simplistic assumption has to be made that the film will rupture at a certain thickness. Even the order of magnitude of the film thickness at rupture is not well agreed upon, with studies reporting thicknesses of 10–50 μm (23), 1–3 μm (8) and 0.1–1 μm (9). Studies using laser interferometry to measure film thickness show that films often thin down to less than 1 μm [11, 21, 26, 27]. Moreover, when rupture occurs, the film may not have uniform thickness. Areas where the film is thinner than others, caused by the formation of a "pimple" or "dimple", have been suggested as being the point of rupture [1, 11, 18]. Squeeze flow models do not consider these phenomena.

While the squeeze flow models have the limitations discussed above, they are advantaged in being simple and having analytical solutions. Experimental coalescence results for identical droplets generally have poor repeatability due to the difficulty in controlling all the factors involved. Therefore using a complex model may not give a better prediction of experimental results than the squeeze flow models. In this work, the coalescence times for biodiesel and glycerol droplets are predicted to an order of magnitude by the squeeze flow equations, providing an insight into film behaviour during thinning.

Retraction of the Thin Film Around the Droplet

Once the film has thinned sufficiently, it ruptures and retracts around the droplet, forming a rim at its edge as illustrated in Fig. 3. One model for the velocity of the rim of the film during retraction assumes that the rim takes on a circular cross-section, as shown in Fig. 4 [28]. The rim is subjected to two opposing forces: (i) the interfacial tension of the two interfaces of the film and (ii) the drag exerted on the rim by the surrounding fluid. The interfacial tension force per unit length is simply 2σ. The drag force per unit length, F_D, is estimated from the drag on a unit length of a rigid cylinder moving through an infinite fluid in the laminar regime, given by [28, 29]:

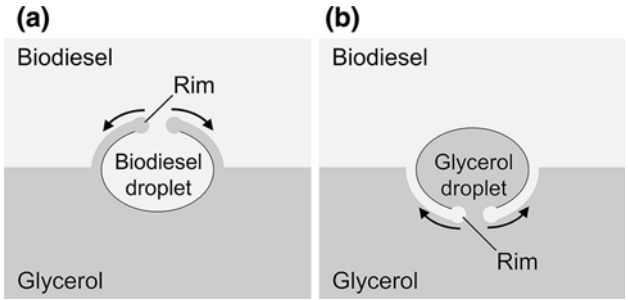

Fig. 3 Schematic diagram of **a** a biodiesel droplet and **b** a glycerol droplet during the retraction of the thin film surrounding the droplet

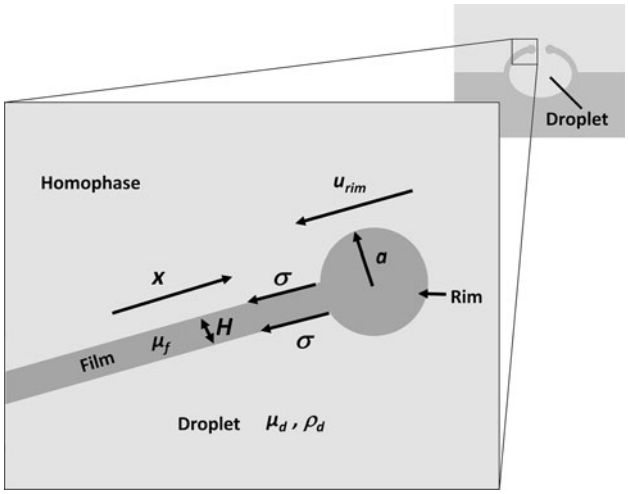

Fig. 4 Schematic diagram depicting the cross-section of a biodiesel droplet during film retraction (*top right*) and a close-up view of the film rim

$$F_D = \frac{4\pi\mu_d u_{rim}}{\ln\left(\frac{4\mu_d}{\rho_c u_{rim} a}\right)} \tag{13}$$

where μ_d and ρ_d are the viscosity and density of the droplet phase surrounding the rim, u_{rim} is the velocity of the rim and a is its cross-sectional radius. Assuming the rim velocity is constant, then the drag force F_D is equal to the interfacial tension force 2σ, yielding:

$$\ln\left(\frac{4\mu_d}{\rho_c u_{rim} a}\right) = \frac{2\pi\mu_d u_{rim}}{\sigma} \tag{14}$$

In Eq. (14) the predominant drag on the rim is assumed to be that exerted by the surrounding fluid. The model neglects any internal drag created by the collection of liquid from within the film into the rim as it progresses. The rim moves with velocity u_{rim} while the film remains stationary. As seen by an observer moving with the rim, liquid from the film flows into the rim with velocity u_{rim} and decelerates within the rim to zero velocity. The flow of liquid from the film into the rim is impeded by internal drag caused by the film's own viscosity.

The internal drag may be accounted for by considering the axial stress p_{xx}, created by the flow of velocity u:

$$p_{xx} = 2\mu_f \frac{du}{dx} - p \tag{15}$$

where du/dx is the strain rate of liquid within the film, μ_f is the viscosity of the film and p is the static pressure [5]. This stress exerts a force on the rim that opposes the interfacial tension force, 2σ. The static pressure p exerts no net force. The drag force of the liquid surrounding the rim is assumed to be negligible, so the force balance per unit length of the rim yields:

$$2\mu_f \frac{du}{dx} H = 2\sigma \tag{16}$$

where H is the film thickness. It is assumed that the fluid within the film has an initial velocity of u_{rim} relative to the rim and decelerates to zero within a distance equal to the film thickness, H. Then the strain rate is given by:

$$\frac{du}{dx} = \frac{u_{rim}}{H} \tag{17}$$

Substituting Eq. (17) into Eq. (16) gives:

$$u_{rim} = \sigma/\mu_f \tag{18}$$

Eq. (14) accounts for the external drag exerted on the rim by the surrounding fluid and does not consider the internal drag created by flow within the film. Conversely, Eq. (18) accounts for the internal drag but not the external drag.

Experimental Procedures

In this work, optical videos were taken of individual biodiesel or glycerol droplets coalescing at a biodiesel/glycerol interface. The time required for film thinning and the velocity at which the film retracted after rupture were measured from the videos.

Manufacture of the Biodiesel and Glycerol Phases

Both the glycerol and biodiesel were produced by the transesterification of rapeseed oil (Holland UK). Transesterification was performed using a methanol reactant (Fisher Scientific) at a 6.2:1 molar ratio of methanol to oil [30]. The catalyst used was sodium methoxide (Fisher Scientific) at a concentration of 1.0 wt% of the rapeseed oil weight. The reaction was carried out in a stirred batch reactor at 50 °C for 60 min. Stirring was provided by a 6-blade Rushton impeller at 800 rpm. To determine the extent of the reaction, a sample of the biodiesel phase was tested by gas chromatography using a standard method [31]. The reaction was thus shown to have converted 97 % of the vegetable oil into esters. Neither the biodiesel nor glycerol phases were treated any further, and so both phases contained impurities, particularly methanol, soaps and unreacted vegetable oil.

Procedure for Video Recording Interfacial Coalescence

The experimental apparatus used to video record the interfacial coalescence of a biodiesel or glycerol droplet is shown in Fig. 5. A square cuvette, 10 mm wide, was filled with a 20-mm deep layer of glycerol at the bottom (being

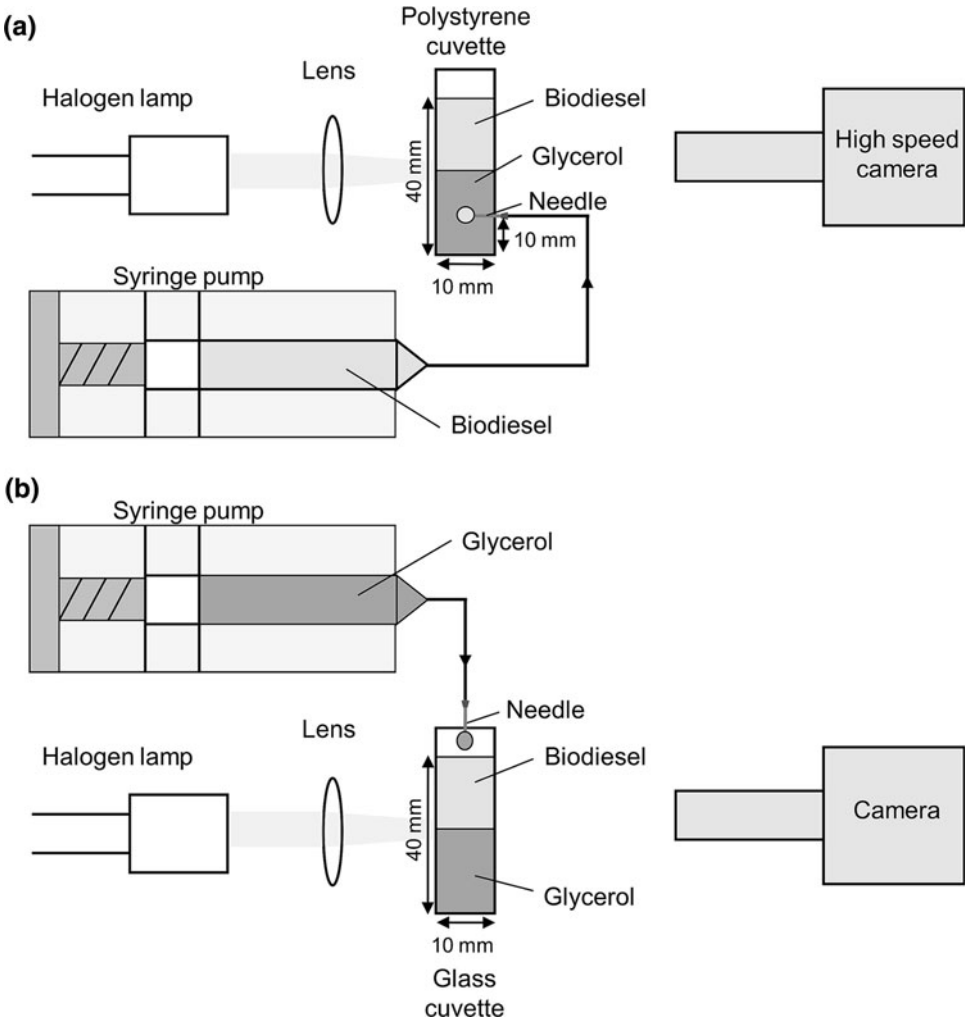

Fig. 5 Apparatus for recording the interfacial coalescence of a biodiesel or glycerol droplet, which are shown here being fed simultaneously but in practice were fed separately into a cuvette

the heavy phase) and another 20-mm deep layer of biodiesel on top. For a biodiesel droplet, a polystyrene cuvette was used with a flat-tipped needle (gauge 18) inserted into the side of the cuvette, 10 mm from the bottom, and connected to a syringe pump filled with biodiesel. The pump was set to 5 ml/h so that a droplet of biodiesel was introduced into the glycerol layer through the needle. When it had reached a critical size, the droplet detached from the needle and rose to the interface between the two phases. At this point the syringe pump was stopped. A high speed CCD camera recorded the droplet's approach to the interface, and its coalescence with the homophase. Back illumination was provided by a halogen light source. Images were taken at 250 frames per second.

The procedure for recording the interfacial coalescence of glycerol droplets was similar to that for biodiesel droplets. However, a glass cuvette was used with a needle (inner diameter 1.2 mm, gauge 16) positioned just above the biodiesel surface (see Fig. 5). Glycerol was fed from the syringe pump at 5 ml/h until the glycerol droplet detached from the needle and sank through the biodiesel layer to the interface. At this point the syringe pump was stopped. The interfacial coalescence of a glycerol droplet was recorded at both 4 and 250 frames per second.

Measurement and Modelling of Film Thinning

Experimental Method for Measuring Film Thinning Times

Figure 6 shows still photographs from the videos of biodiesel and glycerol droplets coalescing at an interface. From these videos, the time required for the thinning of the liquid film around the droplet was measured.

For the biodiesel droplets, the film thinning times were measured from the point at which the droplet was measured to be within 80 microns of the interface, as shown in Fig. 6b, until the point when rupture of the film was visible, as in Fig. 6c. These measurements were accurate to ±0.02 s. For the glycerol droplets, the times were measured from the first frame at which the droplet was

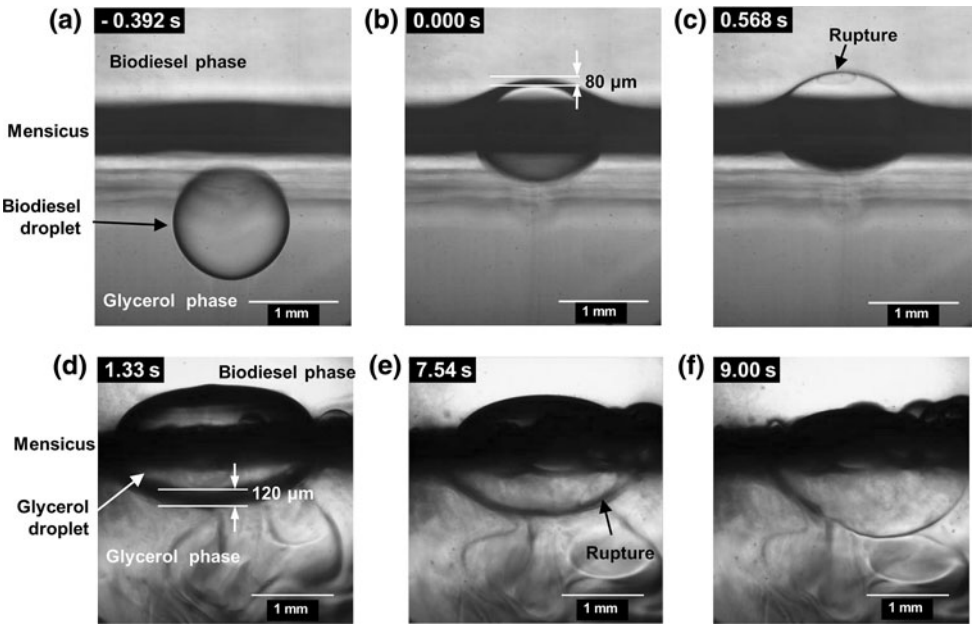

Fig. 6 **a** A biodiesel droplet approaching the interface. **b** The biodiesel droplet when the film thickness was 80 µm, the point at which $t = 0$. **c** The biodiesel droplet when the film has just ruptured. **d** A glycerol droplet soon after falling onto the interface. **e** The glycerol droplet at the point of rupture. **f** The glycerol droplet shortly after rupture during film retraction

positioned on the interface, seen in Fig. 6d, until the frame when film rupture could be seen, as in Fig. 6e. These measurements were accurate to ±0.25 s. The reduced accuracy for glycerol droplets was due to the low frame rate used, which meant that the timing started up to 0.25 s after the droplet landed on the interface. The low frame rate was required to record the entire period of film thinning within the available memory. The resulting error is only around 1 % of the total thinning time. The initial film thickness for glycerol droplets, such as that in Fig. 6d, appeared to be no greater than 120 microns, although it may have been less than this as the curvature of the film made it difficult to gauge an accurate measurement. The experiment was repeated under identical conditions 38 times for biodiesel droplets and 26 times for glycerol droplets.

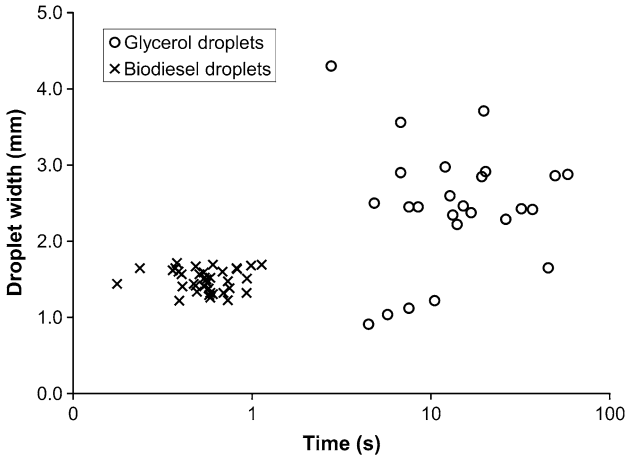

Fig. 7 Film thinning times for biodiesel and glycerol droplets of various sizes

Experimental Results of Film Thinning Times

The film thinning times up to rupture for biodiesel and glycerol droplets are presented in Fig. 7. There was a difference of 1 to 2 orders of magnitude between the film thinning times for biodiesel droplets and glycerol droplets. For biodiesel droplets the film thinning time was almost always less than 1 s, with a mean of 0.58 s, while for glycerol droplets film thinning took between 3 and 60 s, with a mean of 19 s.

The glycerol droplets were larger than the biodiesel droplets because glycerol tended to adhere better to the steel syringe needle than the non-polar biodiesel. However, there is no correlation shown between droplet size and thinning time in Fig. 7, so the size difference cannot fully explain the difference in film thinning times. There was also greater variability in glycerol droplet size. This is because the glycerol droplets did not detach from the needle at a consistent size, perhaps because random mechanical vibrations played a role in the detachment. On some occasions the glycerol droplets broke up on release from the needle, resulting in multiple smaller droplets. While the large variability in droplet size was not ideal, the lack of correlation in Fig. 7 suggests droplet size was not the main factor in determining the film thinning time.

Both biodiesel and glycerol droplets exhibited a wide range of film thinning times, as previous studies have found [9, 10, 24, 25], but the variability was greater for glycerol droplets. It is possible that the biodiesel film around a glycerol droplet, being the less viscous film, was more

susceptible to being ruptured by pimples or dimples formed by perturbations in the fluid. Rupture could therefore take place over a wider range of film thicknesses, resulting in the greater variability in thinning times. Despite the large variability in the data, the difference in film thinning times for biodiesel and glycerol droplets was significant.

The lower film thinning times for biodiesel droplets may appear surprising. A glycerol film around a biodiesel droplet has a high viscosity, so it might be assumed that the film would thin slowly. By the same logic, a low viscosity biodiesel film around a glycerol droplet might thin quickly. However, the opposite result was seen experimentally. An explanation for this is that the biodiesel film around a glycerol droplet experiences the "no slip" boundary condition, resulting in slow thinning, while the glycerol film around a biodiesel droplet experiences "perfect slip" and thins quickly. A diagram of these two modes of film thinning is given in Fig. 8. To determine whether the degree of slip can explain the experimental results, film thinning was modelled for the "perfect slip" and "no slip" boundary conditions.

Squeeze Flow Models for Film Thinning

Film Thinning with No Slip at the Interfaces

The thinning of the biodiesel film around a glycerol droplet (shown in Fig. 8a) was modelled as the squeeze flow of a Newtonian liquid under a constant force with a boundary condition of no slip at the interfaces, using Eq. (5). The force F on the draining film resulted from the buoyancy or weight of the droplet and is given by:

$$F = \Delta\rho g V \tag{19}$$

Where $\Delta\rho$ is the density difference between the droplet and the surrounding phase and V is the droplet volume. The volume V for a glycerol droplet was calculated by assuming it took the shape of an oblate ellipsoid, giving:

$$V = 4\pi b^2 c/3 \tag{20}$$

where $2b$ is width of the droplet and $2c$ is its height. The method for measuring b and c is illustrated in the supplementary material. The film around the droplet follows a curved ellipsoidal surface whose area A is approximately that of a spherical cap:

$$A = 2\pi r_c c \tag{21}$$

where r_c is the radius of curvature and c is the height of the cap, assumed to be equal to half the height of the droplet, (see supplementary material). The squeeze flow model represented by Eq. (5) is for a flat circular film rather than a curved film. The curved film was considered to be equivalent to a flat circle, of radius R, having the same area A as the curved film, so:

$$R = \sqrt{2r_c c} \tag{22}$$

Substituting Eqs. (19), (20) and (22) into Eq. (5) then gives:

$$H(t) = H_0\left(1 + \frac{4H_0^2\Delta\rho g b^2 t}{9\mu_f r_c^2 c}\right)^{-\frac{1}{2}} \tag{23}$$

Film Thinning with Perfect Slip at the Interfaces

The thinning of a glycerol film around a biodiesel droplet was modelled as squeeze flow of a Newtonian liquid under a constant force with perfect slip at the film interfaces, using Eq. (12). The applied force F was calculated from Eq. (19). The volume was calculated from the radius of the droplet before it reached the interface. Figure 6a shows that the droplet was spherical during its approach to the interface. The volume V is then given by:

$$V = 4\pi r_i^3/3 \tag{24}$$

where r_i is the initial radius of the droplet before reaching the interface. The area of the film was obtained from Eq. (21), with r_c and c measured as shown in supplementary

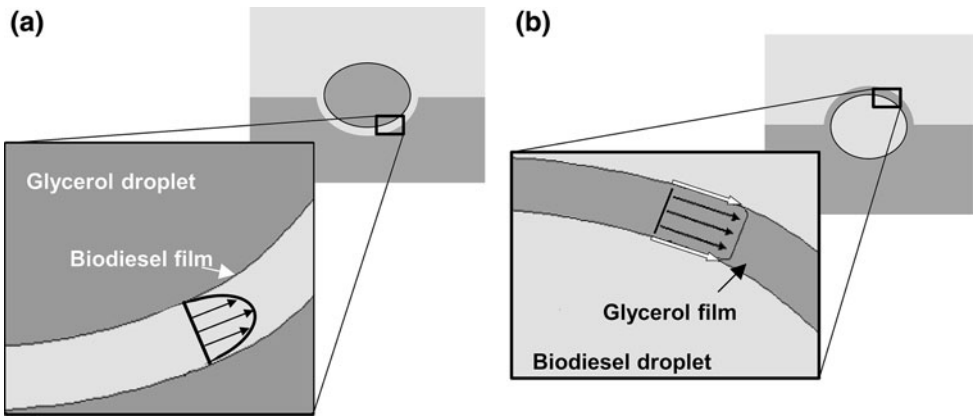

Fig. 8 Modes of film thinning: **a** Thinning of a biodiesel film around a glycerol droplet, where the film interfaces are effectively rigid, allowing no slip. The resulting velocity profile in the film is parabolic, as shown by the *arrows*. **b** Thinning of a glycerol film around a biodiesel droplet with mobile film interfaces allowing slip. The result is a relatively uniform velocity profile

material. Substituting Eq. (19), (21) and (24) into Eq. (12) gives:

$$H(t) = H_0 \exp\left(-\frac{2\Delta\rho g r_i^3 t}{9\mu_f r_c c}\right) \quad (25)$$

Parameter Values and Initial Conditions Used in the Models

To solve Eqs. (23) and (25) several parameters were needed. The densities of biodiesel and glycerol were measured using hydrometers, while the viscosities of biodiesel and glycerol were measured using an ARES rheometer with a Couette cell [32]. The results are shown in Table 1 in the supplementary material.

The droplet dimensions $2b$, $2c$ and r_c were measured for 12 biodiesel droplets and 10 glycerol droplets from photographs (see supplementary material). Additionally, r_i, the initial radius before the droplet reached the interface (see Fig. 6a), was measured for the 12 biodiesel droplets. The mean measurements were used in the model and are tabulated in Table 2 in the supplementary material.

The initial condition for the squeeze flow models is defined by the initial film thickness H_0. For biodiesel droplets H_0 was taken to be 80 μm, based on the distance between the top of the droplet and the interface when the timing of film thinning was started (see Fig. 6b). For glycerol droplets H_0 was taken to be 120 μm, which was the apparent film thickness from the photographs (Fig 6d). However, as an accurate measurement of film thickness was not possible, the sensitivities of the models to H_0 have been examined (see Fig. 9a below).

Results from the Squeeze Flow Models

The equations for squeeze flow with no slip (Eq. (23)) and with perfect slip (Eq. (25)) were solved for three different scenarios.

First, the thinning of a glycerol film around a biodiesel droplet was modelled with perfect slip and with no slip to compare the two models with identical parameters. For each case, four different values of the initial film thickness, H_0, were considered to show the effect of H_0 on the results, which are given in Fig. 9a.

Second, the thinning of a glycerol film around a biodiesel droplet was modelled with perfect slip and the thinning of a biodiesel film around a glycerol droplet was modelled with no slip, as expected for the real droplets. The results are shown in Fig. 9b.

The third scenario also modelled the thinning of a glycerol film around a biodiesel droplet with perfect slip, and the thinning of a biodiesel film around a glycerol droplet with no slip. However, the value of A, the film area, was varied for both cases to show its effect on the results, which are given in Fig. 10. The values chosen for A encompassed the range of film areas that were exhibited by biodiesel and glycerol droplets in the experiments.

The results for the first scenario, which modelled identical biodiesel droplets under conditions of perfect slip and no slip (Fig. 9a), show that when all other parameters were held constant, the slip condition had a very large effect on the kinetics of film thinning. The initial film thickness, H_0, had a relatively small effect on the thinning kinetics compared with the slip condition (see Fig. 9a).

The second scenario, where a biodiesel droplet was modelled with perfect slip and a glycerol droplet with no slip, is given in Fig. 9b, showing that the film thinning for glycerol droplets was much slower than for biodiesel droplets. For a biodiesel droplet with a glycerol film, having perfect slip at the interfaces, the model predicted that the film would reach a thickness of 10 μm in 0.4 s. In contrast, for the glycerol droplet surrounded by a biodiesel film, having no slip at the interfaces, the model predicted that the film would reach a thickness of 10 μm after 78 s. For comparison, the film thinning times measured

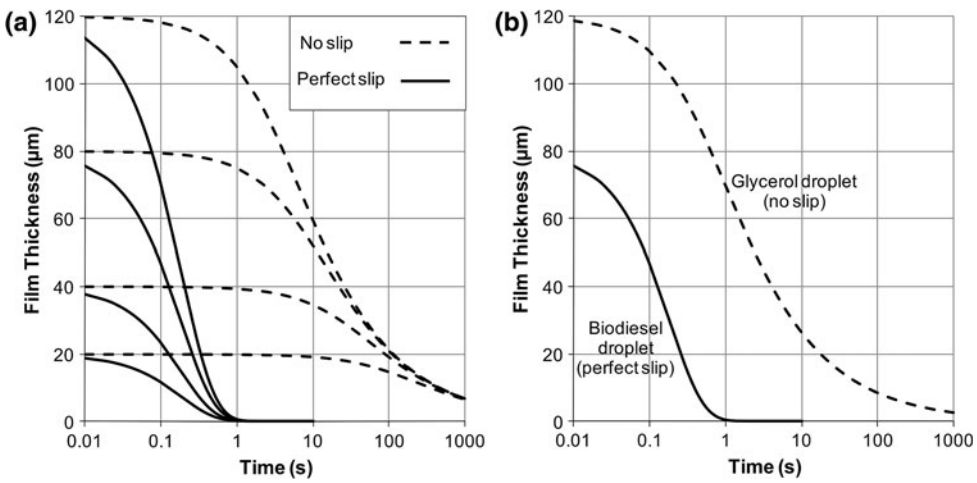

Fig. 9 **a** Solutions for the squeeze flow equations of perfect slip and no slip for a biodiesel droplet with constant dimensions, given in Table 2, for $H_0 = 20$, 40, 80 and 120 microns. **b** Solutions for the squeeze flow equations of perfect slip for a biodiesel droplet with a glycerol film ($H_0 = 80$ μm), and no slip for a glycerol droplet with a biodiesel film ($H_0 = 120$ μm). The dimensions of the biodiesel and glycerol droplets are given in Table 2

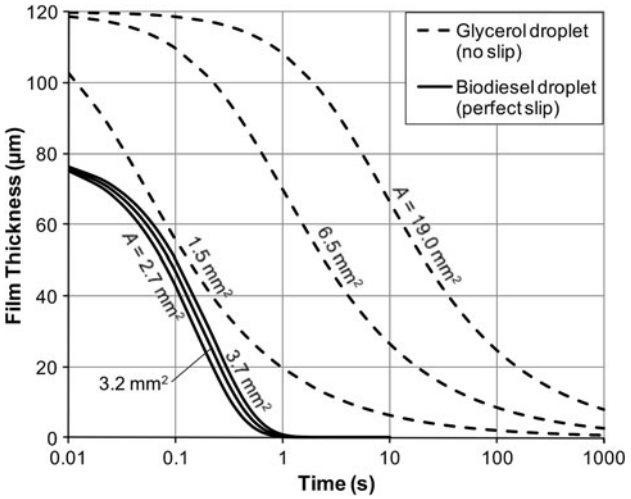

Fig. 10 Solutions for the squeeze flow equations of perfect slip for biodiesel droplets (Eq. (25), solid lines) and no slip for glycerol droplets (Eq. (23), dotted lines). The film area A was varied to determine its effect. The average measured film areas were 3.2 mm^2 for biodiesel droplets and 6.5 mm^2 for glycerol droplets

experimentally were less than 1 s for biodiesel droplets and from 3 to 60 s for glycerol droplets (see Fig. 7). The precise time at which film rupture occurs could not be estimated from the models because film thickness is not the only factor determining film rupture. However, it is assumed that rupture was most likely to occur when the film thickness was less than 10 μm. The predicted times for film thinning to 10 μm were within the same order of magnitude as the experimental times for film thinning.

The results for the third scenario, where the film areas were varied (Fig. 10), show that film area (and hence the droplet size) was predicted to have a significant effect on the film thinning rate. Smaller droplets have reduced film areas and so should result in shorter thinning times according to the model, especially for glycerol droplets, which are modelled using the "no slip" boundary condition. This prediction is important, because in the stirred dispersions of glycerol in biodiesel encountered in industry, the droplet diameters are expected to be from 20 to 200 μm [33], considerably smaller than the droplets investigated here. However, from the experimental results plotted in Fig. (7), there was no apparent correlation of droplet size with the thinning time until film rupture. This discrepancy between model and experiment demonstrates the limits of the squeeze flow models. The squeeze flow models cannot predict the precise time of rupture, as a specific film thickness at which rupture occurs is not known for this system. It was assumed that the film would thin to at least 10 μm before rupture occurred, but in reality rupture for every droplet would not occur at the same uniform film thickness. The optical method used does not provide sufficient resolution to make an accurate measurement of the film thickness at rupture. Laser interferometry would be required, as used in other studies [12, 21, 26, 27], and would provide a useful measure of the accuracy of the squeeze flow models. When the film becomes very thin (<0.1 μm), the effects of electric double layers and van der Waals forces would start becoming important [13] and the squeeze flow model is less applicable. The assumption of uniform film thickness becomes less valid as "dimples" and "pimples" start to form [11, 18]. These pimples, as well as random disturbances in the fluid [9, 18], contribute to rupture by bringing the interfaces close enough for attractive forces to overcome the double layer repulsion. The mechanisms of rupture are not considered in the squeeze flow models and there is uncertainty on the film thickness at rupture.

Another area of uncertainty is the effect of surfactants and other solutes on film thinning, which was not considered in the models. The mass transfer of solutes can enhance film thinning [15–17]. The biodiesel and glycerol phases were well mixed during the transesterification process, and so will have achieved equilibrium. Mass transfer should therefore have been negligible. Surfactant components within the film, however, may have inhibited film thinning due to the Marangoni effect [13, 18, 19, 21]. The presence of surfactants was indicated by the very low interfacial tension of the system, which was measured by the du Noüy ring method as 0.6 mN/m. During transesterification, saponification side reactions occur between the fatty acids and potassium hydroxide, which is used as a catalyst [34]. The resulting soaps may be expected to remain preferentially in the glycerol, being the polar phase. Therefore, a glycerol film surrounding a biodiesel droplet should thin more slowly due to the presence of soaps. In fact, the opposite was seen in the experiments, with the glycerol film thinning quickly compared to the biodiesel film. The rapid thinning of the glycerol film seems to contradict the widely held view that surfactants in the film invariably lead to no slip at the interface [11–13].The matter is complicated by the presence of other surfactants in the biodiesel phase, namely mono- and diglyceride intermediate products. A standard gas chromatograph analysis [31] of the biodiesel phase found concentrations of 1.2 wt% monoglycerides and 0.4 wt% diglycerides. Analysis of soap content in the glycerol phase was not performed and it is difficult to predict which surfactants might have had a greater inhibiting effect on film thinning. While it is not clear what role surfactants played in the biodiesel/glycerol system, there is also no obvious way that surfactants may have caused the large difference in film thinning behaviour for biodiesel and glycerol films. The difference in slip conditions at the interface remains the most likely explanation.

The cases of perfect slip and no slip boundary conditions are extreme scenarios; in reality partial slip may occur in

most cases. But the fact that the predicted kinetics of film thinning are in approximate agreement with observed film thinning times shows that the relative degree of slip at the interface explains the difference in rupture times between biodiesel and glycerol droplets. While no slip and perfect slip boundary conditions have been applied previously to film thinning [6, 12], this is the first time that they have both been used to explain experimental results.

Measurement and Modelling of Film Retraction

Experimental Method of Measuring the Rim Velocity during Film Retraction

High speed videos of biodiesel and glycerol droplets coalescing at a biodiesel/glycerol interface were recorded, as detailed in the Sect. "Procedure for Video Recording Interfacial Coalescence", at 250 frames per second. Single frames from the videos are given in Fig. 11.

Biodiesel and glycerol produced by transesterification were contaminated by surfactants and so were not ideal fluids for testing the models for rim velocity. Alternate model fluids with well defined properties were therefore used in addition to biodiesel and glycerol. The model fluids were polydimethylsiloxane (PDMS, Sigma Aldrich) and an aqueous glycerol solution made up of 50 % pure laboratory grade glycerol (Fischer Scientific) in distilled water. To distinguish the two types of glycerol used in these experiments they will be referred to as crude glycerol, being glycerol produced by transesterification, and aqueous glycerol, being the model fluid. Experiments on model fluids were conducted by the same method as described in Sect. "Procedure for Video Recording Interfacial Coalescence"

In the photographs in Fig. 11, the rim of the retracting film is just visible. The velocity of the rim was determined by measuring the distance that the rim travelled between successive frames in the video. The rim retraction was rapid but proceeded smoothly without the formation of satellite droplets, as can be seen in Fig. 11. Details of the measurement method are provided in the supplementary material.

Experimental Results and Model Predictions for the Rim Velocity During Film Retraction

The results of the rim velocity measurements for four different droplet types are shown in Fig. 12 and the data are given in Table 3 in the supplementary material. The rim for a biodiesel droplet moved faster than the rim for a glycerol droplet. This result can be explained in terms of the drag force experienced by the rim. For a biodiesel droplet the film rim was surrounded by biodiesel (see

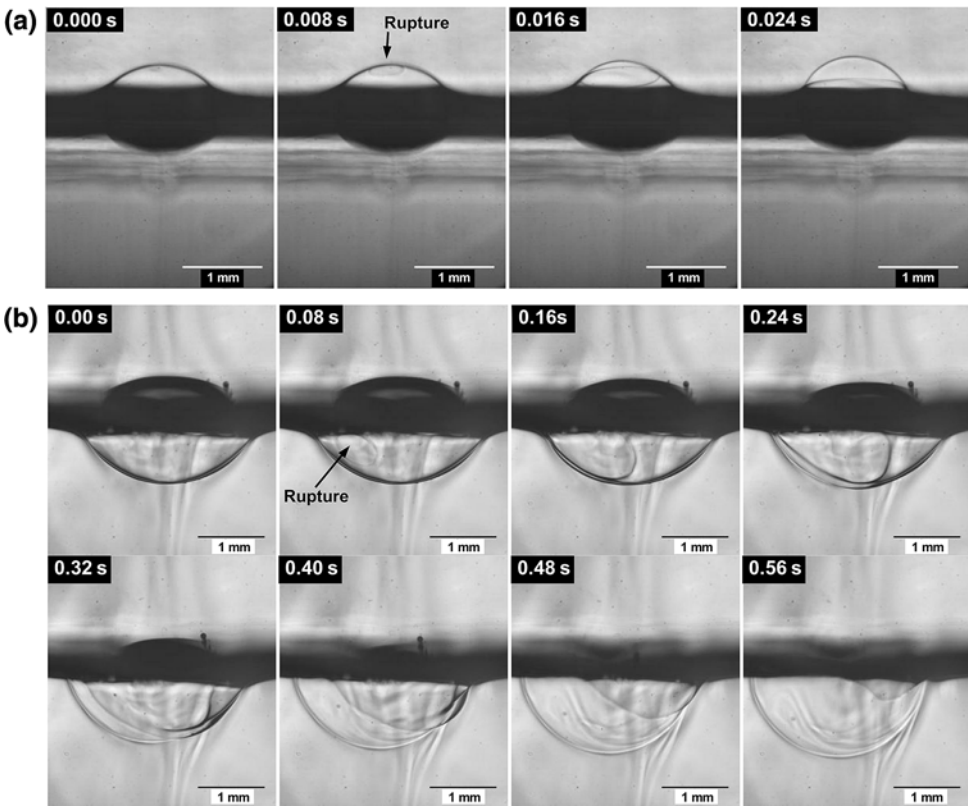

Fig. 11 Still photographs at the biodiesel/glycerol interface during film retraction for **a** a biodiesel droplet and **b** a glycerol droplet

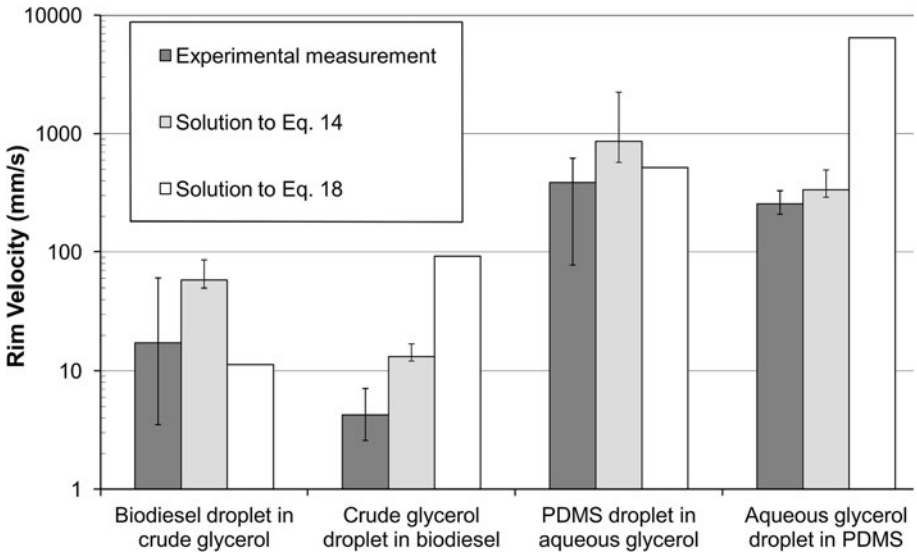

Fig. 12 Experimental measurements of rim velocities compared with predictions from Eqs. (14) and (18) for four types of droplet. The *error bars* show the range of experimental measurements and, for Eq. (14), the effect of varying rim radius a from 1 to 20 μm

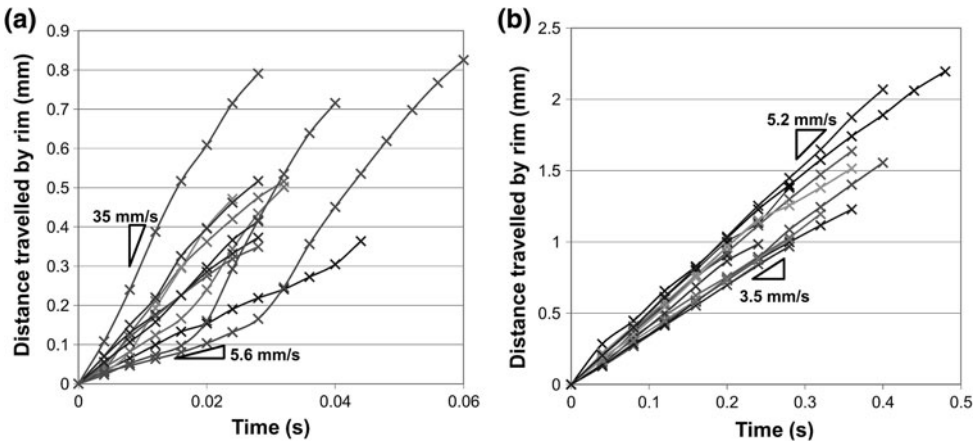

Fig. 13 Plots of the distance travelled by the rim as a function of time for **a** biodiesel droplets and **b** crude glycerol droplets. Each line represents the rim on a single droplet

Fig. 3), which is relatively inviscid. Therefore the rim experienced little drag. For a glycerol droplet the film rim was surrounded by viscous glycerol, which exerted a greater drag on the rim. Therefore the rim for a glycerol droplet moved more slowly than the rim for a biodiesel droplet. The rim velocities for PDMS and aqueous glycerol droplets were much higher than those for biodiesel and crude glycerol droplets because the PDMS/aqueous glycerol system had a much higher interfacial tension than the biodiesel/crude glycerol system (see Table 5). Both Eqs. (14) and (18) take account of the interfacial tension, resulting in corresponding increases in the predicted rim velocities for the PDMS/aqueous glycerol system compared with the biodiesel/crude glycerol system.

The error bars for the experimental results in Fig. 12 depict the maximum and minimum measured velocities. There was large variability in the measured rim velocities, particularly for biodiesel droplets and PDMS droplets, which both had a viscous film surrounded by a less viscous fluid. The reason for this variability is not known, but it is possible that as the film retraction was controlled by internal flow, the rim velocity was more susceptible to minor impurities in the film. The variability in rim velocities is illustrated in Fig. 13, which shows the distance travelled by the rim as a function of time for some of the biodiesel and glycerol droplets that were studied. The slopes of the plots indicate the rim velocity. For biodiesel droplets there was much variability in the rim velocity, as shown by the variety of gradients in Fig. 13a. Some of the individual lines in Fig 13a change gradient markedly, indicating that even on a single droplet the rim velocity may change over time. There was much less variability for glycerol droplets, as shown in Fig. 13b; the curves are nearly linear and the range of gradients is much less than for the biodiesel droplets.

The rim velocities for the four different types of droplet were predicted by Eqs. (14) and (18). Equation (14) was solved numerically for u_{rim} using the Solver function in Microsoft Excel. The parameters used in the model equations are given in Table 4 in the supplementary material.

The results are given, together with the mean rim velocities measured experimentally, in Fig. 12 and also in Table 6 in the supplementary material.

Figure 12 shows that Eq. (18) was better at predicting the rim velocity for biodiesel droplets in crude glycerol and PDMS droplets in aqueous glycerol. In both of these cases, the film was of higher viscosity than the surrounding liquid. The internal resistance to flow within the rim dominated, so Eq. (18) was appropriate. For the crude glycerol droplet in biodiesel and the aqueous glycerol droplet in PDMS, the film was of lower viscosity than the surrounding fluid. In these cases the external drag on the rim dominated, so Eq. (14) was appropriate.

In using Eq. (14), several simplifying assumptions had to be made. First, the rim velocity was assumed to be constant so that acceleration was not included in the force balance. The rim radius, a, was also assumed to be constant when in reality it would increase as it gathered a greater quantity of fluid. There was uncertainty in the value of a, as the rim radius was not measured. Therefore an assumed value of 10 μm was used for all types of droplet. The error bars in Fig. 12 show the range of results obtained from Eq. (14) when the value of a was varied from 1 μm up to 20 μm. This is the best estimate for the range of a based on images from the videos, which show the rim to be visible but of very small radius. The effect of a on the rim velocity that resulted from Eq. (14) is shown in Fig. 14. The error bars in Fig. 12 suggest that the effect of varying a was small compared to the effect of changing the model from considering external to internal drag. These simplifications, inherent to Eq. (14), and the fact that internal drag was neglected, help to explain why Eq. (14) overestimated the rim velocities. However, Eq. (14) came closer to predicting the experimental results when the fluid surrounding the rim was viscous, demonstrating that in this case external drag had a greater effect on the rim velocity than internal drag.

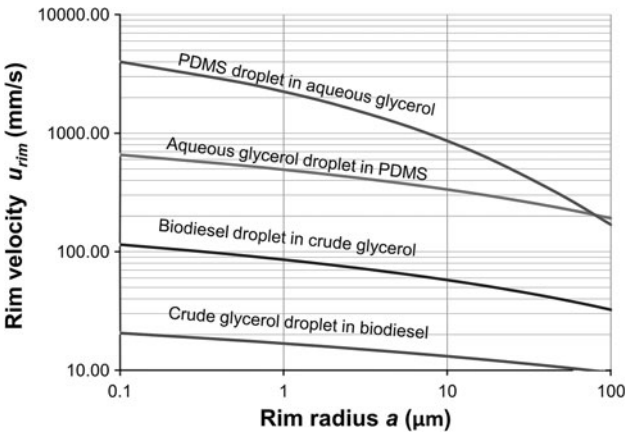

Fig. 14 Plot showing the dependence of the rim velocity u_{rim} on the rim radius a, as calculated by Eq. (14)

Implicit within the film retraction models is the assumption of laminar flow conditions. To validate this assumption, a film Reynolds number may be defined as:

$$\mathrm{Re} = \rho_f u_{rim} a / \mu_f \quad (26)$$

The Reynolds numbers for each type of droplet are provided in Table 5 in the supplementary material. In all cases the Reynolds number was less than one, confirming the laminar flow assumption.

Conclusions

Two stages in the coalescence of a single biodiesel or glycerol droplet at a biodiesel/glycerol interface have been investigated, namely: the thinning of the liquid film between the droplet and its homophase; and the retraction of the film around the droplet after rupture.

The time required for the film surrounding the droplet to thin and rupture differed greatly for biodiesel and glycerol droplets, with glycerol droplets taking 1–2 orders of magnitude more time. In the case of the biodiesel drop, the trapped film of glycerol was surrounded on both sides by low viscosity biodiesel, providing the equivalent of slip conditions at the film boundaries. The thinning of the film was then only controlled by weak extensional viscosity effects. In the case of the glycerol droplet, the trapped film of biodiesel was surrounded by viscous glycerol, providing essentially a no slip boundary condition at the interfaces, resulting in simple shear flow and a viscous resistance to thinning. The boundary conditions of the flow played a greater role on the thinning process than the viscosity of the trapped liquid itself.

Observations of film retraction showed that the film around a biodiesel droplet retracted faster than the film around a glycerol droplet. This difference can be explained by the external drag exerted by the surrounding fluid on the film as it retracted. For a biodiesel droplet, the film was surrounded by low viscosity biodiesel, which exerted little drag on the rim of the film. The retraction velocity in this case was best modelled by balancing the internal drag due to viscosity within the film with interfacial tension. For a glycerol droplet, the film was surrounded by glycerol of high viscosity, which exerted substantial drag on the rim. For this scenario the retraction velocity was best modelled by balancing the external drag on the film with interfacial tension.

The results reported in this paper are of particular relevance to glycerol separation for biodiesel production. However, glycerol concentrations in commercial biodiesel manufacture are typically 20 % by volume, so concentration effects will also influence coalescence kinetics. The work reported here is also of general relevance to

immiscible systems with similar viscosities and interfacial tension to those considered in this paper. The theoretical modelling can be used for calculation of kinetics for other systems.

Acknowledgments AA would like to thank the William Georgetti Trust and Cambridge Commonwealth Trust for financial support to carry out this work.

References

1. Frising T, Noik C, Dalmazzone C (2006) The liquid/liquid sedimentation process: from droplet coalescence to technologically enhanced water/oil emulsion gravity separators: a review. J Dispers Sci Technol 27:1035–1057
2. Zhou W, Boocock DGB (2006) Phase behaviour of the base-catalyzed transesterification of soybean oil. J Am Oil Chem Soc 83:1041–1045
3. Engmann J, Servais C, Burbidge AS (2005) Squeeze flow theory and applications to rheometry: a review. J Non-Newtonian Fluid Mech 132:1–27
4. Reynolds O (1886) On the theory of lubrication and its application to Mr. Beauchamp Tower's experiments, including an experimental determination of the viscosity of olive oil. Philos Trans R Soc Lond 177:157–234
5. Kay JM, Nedderman RM (1985) Fluid mechanics and transfer processes. Cambridge University Press, Cambridge
6. Jeelani SAK, Hartland S (1994) Effect of interfacial mobility on thin film drainage. J Colloid Interface Sci 164:296–308
7. Chesters AK (1991) The modelling of coalescence processes in fluid-liquid dispersions: a review of current understanding. Chem Eng Res Des 69:259–270
8. Gillespie T, Rideal EK (1955) The coalescence of drops at an oil-water interface. Trans Faraday Soc 52:173–183
9. Charles GE, Mason SG (1960) The coalescence of liquid drops with flat liquid/liquid interfaces. J Colloid Sci 15:236–267
10. Chan DYC, Klaseboer E, Manica R (2011) Film drainage and coalescence between deformable drops and bubbles. Soft Matter 7:2235–2264
11. Klaseboer E, Chevaillier JP, Gourdon C, Masbernat O (2000) Film drainage between colliding drops at constant approach velocity: experiments and modelling. J Colloid Interface Sci 229:274–285
12. Yeo LY, Matar OK, Perez de Ortiz ES, Hewitt GF (2003) Film drainage between two surfactant-coated drops colliding at constant approach velocity. J Colloid Interface Sci 257:93–107
13. Kumar K, Nikolov AD, Wasan DT (2002) Effect of film curvature on drainage of thin liquid films. J Colloid Interface Sci 256:194–200
14. Chevaillier JP, Klaseboer E, Masbernat O, Gourdon C (2006) Effect of mass transfer on the film drainage between colliding drops. J Colloid Interface Sci 299:472–485
15. Ban T, Kawaizumi F, Nii S, Takahashi K (2000) Study of drop coalescence behaviour for liquid–liquid extraction operation. Chem Eng Sci 55:5385–5391
16. Marucci G (1969) A theory of coalescence. Chem Eng Sci 24:975–985
17. Ivanov IB, Kralchevsky PA (1997) Stability of emulsions under equilibrium and dynamic conditions. Colloids Surf A 128: 155–175
18. Rommel W, Meon W, Blass E (1992) Hydrodynamic modelling of droplet coalescence at liquid–liquid interfaces. Sep Sci Technol 27:129–159
19. Hodgson T, Lee JC (1969) The effect of surfactants on the coalescence of a drop at an interface I. J Colloid Interface Sci 30: 94–108
20. Hodgson T, Woods DR (1969) The effect of surfactants on the coalescence of a drop at an interface II. J Colloid Interface Sci 30:429–446
21. Henschke M, Schlieper LH, Pfennig A (2002) Determination of a coalescence parameter from batch-settling experiments. Chem Eng J 85:369–378
22. Hartland S (1967) The coalescence of a liquid drop at a liquid–liquid interface Part II: film thinning. Trans Inst Chem Eng 45:102–109
23. Cockbain EG, McRoberts TS (1953) The stability of elementary emulsion drops and emulsions. J Colloid Sci 8:440–451
24. Watanabe T, Kusui M (1958) On the mechanism of the coalescence of drops at an oil–water interface. Bull Chem Soc Jpn 31:236–243
25. Burrill KA, Woods DR (1973) Film shapes for deformable drops at liquid–liquid interfaces II: the mechanisms of film drainage. J Colloid Interface Sci 42:15–34
26. Zdravkov AN, Peters GWM, Meijer HEH (2003) Film drainage between two captive drops: PEO–water in silicon oil. J Colloid Interface Sci 266:195–201
27. Hartland S (1967) The coalescence of a liquid drop at a liquid–liquid interface Part III: film rupture. Trans Inst Chem Eng 45:109–114
28. Bairstow L, Cave BM, Lang ED (1923) The resistance of a cylinder moving in a viscous fluid. Philos Trans R Soc Lond A 223:383–432
29. Freedman B, Pryde EH, Mounts TL (1984) Variables affecting the yields of fatty esters from transesterified vegetable oils. J Am Oil Chem Soc 61:1638–1643
30. EN 14105 (2003) Fat and oil derivatives—fatty acid methyl esters (FAME) —Determination of free and total glycerol and mono-, di-, triglyceride contents (Reference method). European Committee for Standardisation, Brussels
31. Macosko CW (1994) Rheology: principles, measurements and applications. Wiley-VCH, New York
32. Abeynaike A, Sederman AJ, Khan Y, Johns ML, Davidson JF, Mackley MR (2012) The experimental measurement and modelling of sedimentation and creaming for glycerol/biodiesel droplet dispersions. Chem Eng Sci 79:125–137
33. Mittelbach M, Remschmidt C (2004) Biodiesel: the comprehensive handbook. Martin Mittelbach, Graz, Austria